Manuscript for: **Industrial & Engineering Chemistry Research**

Solvent extraction process for refining cobalt and nickel from a "bulk hydroxide precipitate" obtained by bioleaching of sulfidic mine tailings

Thomas Abo Atia[†]*, Clio Deferm[†], Lieven Machiels[†], Mohammad Khoshkhoo[††], Sofia Riaño[†], Koen Binnemans[†]

[†] KU Leuven, Department of Chemistry, Celestijnenlaan 200F, P.O. box 2404, B-3001 Leuven, Belgium.

[††] Boliden Mineral AB, Fällforsvägen 4, SE-936 81 Boliden, Sweden

*Corresponding author:
Email: thomas.aboatia@kuleuven.be

ORCID:

Thomas Abo Atia: 0000-0002-9744-3195

Clio Deferm: 0000-0003-4550-9567

Lieven Machiels: 0000-0002-0371-424X

Mohammad Khoshkhoo: 0000-0002-3255-3051

Sofia Riaño Torres: 0000-0002-1049-6156

Koen Binnemans: 0000-0003-4768-3606

Abstract

A flowsheet with different solvent extraction (SX) units was tested to purify cobalt, nickel, copper (and zinc) from a so-called "bulk hydroxide precipitate" (BHP) from bioleaching of sulfidic tailings. A complex pregnant leaching solution (PLS) was obtained by sulfuric acid leaching of the BHP, dissolving target (>99.5%) and secondary elements (including silicon). A solvent extraction step with the chelating extractant LIX 984 was integrated into conventional Co-Ni SX refining, separating copper selectively (>99%). Subsequently, di(2-ethylhexyl)phosphoric (D2EHPA) followed by phosphinic acid (Cyanex 272) SX enabled impurity removal and cobalt separation (77%) from nickel and magnesium, respectively. Silica gel was observed in the aqueous raffinate after the Cyanex 272 SX. Dissolved silica involvement in crud/precipitate/gel formation depended on its speciation (polymerization, surface groups) during SX (pH, saponification). Interference by silica was mitigated until cobalt recovery. However, nickel could be separated with the carboxylic Versatic Acid 10 from magnesium only after silica gel filtration, as crud/precipitate formed during SX at pH 7. Advanced ultrasound-assisted antisolvent crystallization gave pure monohydrated $CoSO_4$ and $NiSO_4$.

Keywords: Cobalt; Hydrometallurgy; Nickel; Solvent extraction; Sulfidic tailings

1. Introduction

The supply risk of energy-transition metals used in low-carbon technologies i.e. photovoltaics, wind turbines, electrolysis for green hydrogen, batteries, accumulators, capacitors, etc. may restrain the societal transition towards a circular and climate-neutral economy.[1]

The current mining and refining activities are not able to cope with the huge demand for metals for the energy transition.[2,3] Despite metal recycling rates might improve in the coming years, in the case of fast-growing markets e.g. Li-ion batteries metals, not even 100% of metal recycling might be a timely solution for these high-risk supply materials (e.g. cobalt, nickel, etc.).[4]

Therefore, underexploited resources such as sulfidic tailings might be a valuable, responsible source of energy-transition metals.[5] Sulfidic tailings may cause environmental issues such as acid mine drainage.[6,7] Yet, they may contain exploitable concentrations of valuable metals.[8,9] However, economically feasible and sustainable processes need to be developed for metal extraction from these resources. Low-intensity leaching approaches are gaining the mining industry's attention for recovering metals from low-grade ores and tailings,[10,11] such as bio-leaching, a promising technology to leach metals from sulfidic tailings.[9,12]

Because of the low concentrations of metals in the bioleaching stage, downstream processing might include a precipitation step to concentrate the leached metals in solid intermediates, often in the form of *mixed hydroxide precipitate* MHP or *mixed sulfide precipitate* MSP.[13] These intermediates are further processed to recover valuable metals.[14,15] Distinct downstream purification may be applied, including selective oxidation and/or precipitation, which may be combined with *solvent extraction* (SX).[13,16–23] The more practical solutions adopted by the mining industry might rely on chemical precipitations e.g. sulfide

precipitations, achieving metal sulfides and/or mixed metal sulfides (e.g. Ni/CoS) products.[24] However, SX-based flowsheets provide the advantage of selectively separating metals from complex aqueous solutions, achieving high-degree of separation, which may reflect in high0-purity products, craved by the modern industry e.g. battery materials.[25,26]

Notwithstanding large efforts made to develop thermodynamic models for the predictive modeling of SX equilibria, the development of actual SX processes still relies on extensive experimental lab-scale and piloting work.[27,28]

Thus, the purpose of this study was to validate a SX-based flowsheet to obtain cobalt(II) and nickel(II) sulfates from a special intermediate, herein referred to as *bulk hydroxide precipitate* BHP obtained from bioleaching of sulfidic mine tailings. The acronym BHP was used to differentiate the intermediate used in this study from the conventional MHP intermediate. As intended in the metallurgical industry, the MHP is a rather standardized intermediate, mostly composed of Ni and minor Co as hydroxides, with minimal other impurities (*i.e.* $Mg(OH)_2$),[18] whereas the intermediate used in this work exhibits higher concentrations of Co than Ni and also includes Cu, Zn, and gypsum, as it was obtained by slacked lime precipitation. Cu and Zn might provide supplementary revenue, exploiting the full economic potential in the tailings.

First, the leaching in sulfuric acid was performed in a 5 L reactor to produce a sufficient amount of PLS for studying the downstream operations. A rather conventional SX flowsheet for Co and Ni purification, using in order D2EHPA, Cyanex 272, and Versatic Acid 10 SX, was innovated with a first LIX 984 SX to recover selectively Cu from the PLS, before the other elements separation, directly at the spontaneous PLS pH. For D2EHPA and Cyanex 272 SX, batch countercurrent simulations were performed to mimic these processes in continuous mode. Furthermore, the co-extracted impurities were removed from the cobalt-loaded Cyanex 272 and

the nickel-loaded Versatic Acid 10 organic phases via crosscurrent scrubbing. After stripping, the purified cobalt and nickel were recovered as sulfates by a fast advanced antisolvent crystallization method, enhanced by ultrasounds.

A combination of traditional and innovative (e.g. Cu recovery, antisolvent crystallization) hydrometallurgical operations has been considered to run an exploratory lab-scale flowsheet to benchmark the potential achievements and limitations to directly obtain battery metals from a hydroxide precipitate obtained after bioleaching of sulfidic tailing. A proper reuse of high-sulfur tailings is of timely interest to the metallurgical industry dealing with concerning reclamation of land for safe disposal and risk of secondary pollution.

2. Experimental

2.1 Chemicals

Hydrochloric acid (37%), di(2-ethylhexyl)phosphoric acid (D2EHPA, 95%), *n*-dodecane (99%), and petroleum ether (pure) were purchased from Acros Organics. Nitric acid (65%), and ICP-OES metal standards were from ChemLab. Sulfuric acid (≥ 95%), sodium hydroxide (analytical grade, pearls), and acetone (≥ 99.5%) were purchased from Fisher Scientific. Versatic Acid 10 (> 90%) was obtained from Hexion, bis-(2,4,4-trimethylpentyl)phosphinic acid (Cyanex 272, 85–90%) was obtained from Solvay, LIX 984 (5-nonylsalicylaldoxime/2-hydroxy-5-nonylacetophenone oximes 1:1) was obtained from BASF, and GTL GS190 solvent (C10-13 branched alkanes) was supplied by Shell. $CoSO_4 \cdot 7H_2O$ (≥ 99%) and $NiSO_4 \cdot 6H_2O$ (≥ 99%) from Merck were dehydrated to be compared with the obtained cobalt and nickel sulfates obtained from the BHP. All chemicals were used as received without any further purification unless specified.

BHP was kindly provided by Boliden Mineral AB, Sweden, and was produced during the operation of a pilot scale bioleaching plant (100 kg/day) in which a pyritic tailing that contained

varying amounts of Cu, Zn, Ni, and Co (as sulfides) was used as feed. After bioleaching, the PLS was treated for the removal of iron and arsenic by limestone addition. A two-stage precipitation process was operated at pH 7.9 – 8.6 by the addition of slacked lime ($Ca(OH)_2$) to the purified PLS, precipitating all metals into the intermediate bulk hydroxide precipitate (BHP), which was separated from the barren solution by thickening and filtration.

2.2 Metal determination and quantification

All solids were digested by *i*) microwave digestion at 210 °C (0.25 g of BHP in 5.5 mL of HCl, 2 mL of HNO_3, 0.5 mL of HBF_4) or *ii*) *aqua regia* (HCl: HNO_3 3:1 *vol.*, L/S= 10 mL/1 g BHP or residue) digestion at 70 °C before volumetric dilutions and ICP-OES analysis. Metal concentrations were measured in aqueous and organic solutions by ICP-OES (AVIO 500, Perkin-Elmer). The samples were adequately diluted within the calibration limits (0–10 mg L^{-1}) in 2–5% HNO_3 or *n*-dodecane, and lutetium or rhodium was added as internal standard, respectively. Metal quantification was used for the calculation of the leaching, extraction, and stripping efficiencies (%) as well as the distribution ratios (D_M) according to equations (1), (2), (3), and (4) respectively.

$$Leaching\ efficiency\ (\%) = \frac{C_{M\ leach} \cdot V_{leach}}{m_{M\ BHP}}\% \quad (1)$$

$$Extraction\ (\%) = \frac{C_{M\ org} \cdot V_{M\ org}}{(C_{M\ org} \cdot V_{org} + C_{M\ aq} \cdot V_{aq})}\% \quad (2)$$

$$Stripping\ (\%) = \frac{C_{M\ aq} \cdot V_{aq}}{(C_{M\ org} \cdot V_{org} + C_{M\ aq} \cdot V_{aq})}\% \quad (3)$$

$$D_M = \frac{C_{M_{org}}}{C_{M_{aq}}} \quad (4)$$

2.3 BHP leaching

Preliminary small-scale experiments (1–5 g) were performed in glass vials under magnetic stirring (600 rpm) to optimize the sulfuric acid concentration (0.25–1.5 mol L^{-1}), L/S ratio (5–10), leaching time (1–4 h) and temperature (25–75°C). The optimized leaching conditions were reproduced in 1 L and 5 L reactors (*HiTec Zang)* integrated with vacuum filtration setup, temperature, pH, and ORP control. Filter cakes were washed with a water-equivalent of about 10% of the leaching volume. The leachate and washing waters were combined as starting solutions for the SX experiments.

2.4 SX batch experiments

Batch SX experiments were carried out in screw-cap vials (4–40 mL) and separating funnels (0.1–1.0 L) at room temperature, using 5–30 min shaking (*RS-1 ReciproShaker* or *Burrel Wirst-Action Shaker 95)*. LIX 984 organic phases were prepared in petroleum ether as diluent. D2EHPA, Cyanex 272, and Versatic Acid 10 organic phases were prepared in GS190 diluent and pre-equilibrated with MilliQ® water.[29] Extractants' structures are reported in SI (figure S1). Extraction (equilibrium) pHs were adjusted with aliquots of 10 mol L^{-1} NaOH solutions or by saponification of the organic phase. Countercurrent simulations (see SI, Figure S2, S3) were carried out to assess the metal distributions at promising conditions for D2EHPA and Cyanex 272, simulating continuous processes at O/A= 1.

To scrub impurities from metal-loaded organic phases of Cyanex 272 and Versatic Acid 10, crosscurrent scrubbing (see SI, Figure S4) was performed using cobalt and nickel sulfate solutions (0.5 mol L^{-1}) at an O/A= 20. Finally, the metals were stripped from the metal-loaded organic phases using sulfuric acid solutions ($[H_2SO_4]$= 0.1–4 mol L^{-1}, O/A= 1).

FTIR measurements were carried out on specimens from SX experiments, using a *Bruker Vertex 70 FTIR spectrometer* equipped with the Platinum ATR.

2.5 Antisolvent crystallization of $CoSO_4 \cdot H_2O$ and $NiSO_4 \cdot H_2O$

Monohydrate cobalt and nickel sulfates, $CoSO_4 \cdot H_2O$ and $NiSO_4 \cdot H_2O$, were crystallized from the stripping solution of cobalt-loaded and nickel-loaded aqueous phases. Stripping was quantitative in sulfuric acid (0.6 mol L^{-1}, O/A= 1). An excess of acetone (A/O= 6) was added as an antisolvent. The resulting slurries were placed for 30 s in a sonicated water bath (*Bandelin Sonorex*) to enhance the crystallization.[30] Subsequently, the supernatant was removed after centrifugation (2000 rpm, 2 min). Cobalt(II) sulfate and nickel(II) sulfate were dried overnight at 60 and 175 °C, respectively. The X-ray powder diffractograms (D2 Phaser, Bruker) of the obtained sulfates were compared with those of $CoSO_4 \cdot 7H_2O$ and $NiSO_4 \cdot 6H_2O$ dehydrated at the same drying conditions as the respective products. The metal composition was determined after digestion and ICP-OES analysis and these values were used to calculate the purity of the solids, via equation (5).

$$Purity\ (\%) = \frac{mass\ Co/Ni\ (obtained\ product)}{mass\ Co/Ni\ (theoretical\ product)}\ \% \qquad (5)$$

3. Results and discussion

3.1 Conceptual flowsheet

The conceptual hydrometallurgical flowsheet is shown in Figure 1, starting from BHP leaching and followed by four distinct SX circuits for the recovery of copper and zinc, as well as the cobalt(II) and nickel(II) sulfate, exploiting the selectivities of LIX 984, D2EHPA, Cyanex 272, and Versatic Acid 10 extractants.[31,32] These are acidic extractants operating according to a general cation exchange equilibrium (6):

$$M^{n+} + n\overline{RH} \rightleftharpoons \overline{MR_n} + nH^+ \qquad (6)$$

The objective was to develop a multistage SX process for metal separation from BHP, using the most established acidic extractants, currently applied in mining and battery recycling. Distinctly from most common SX-based flowsheets to recover Co and Ni, a consolidated

technology, applying LIX 984 to selectively remove Cu, was inserted, as the first separation, before the more traditional sequence of SX operations, namely D2EHPA, Cyanex 272, and Versatic acid 10 SX. The flowsheet includes scrubbing and stripping operations, commonly included in standard SX circuits. An innovative method was considered for cobalt and nickel product recovery, obtaining the respective monohydrated sulfates via ultrasound-assisted antisolvent crystallization. The different unit operations of the flowsheet will be described in the following sections.

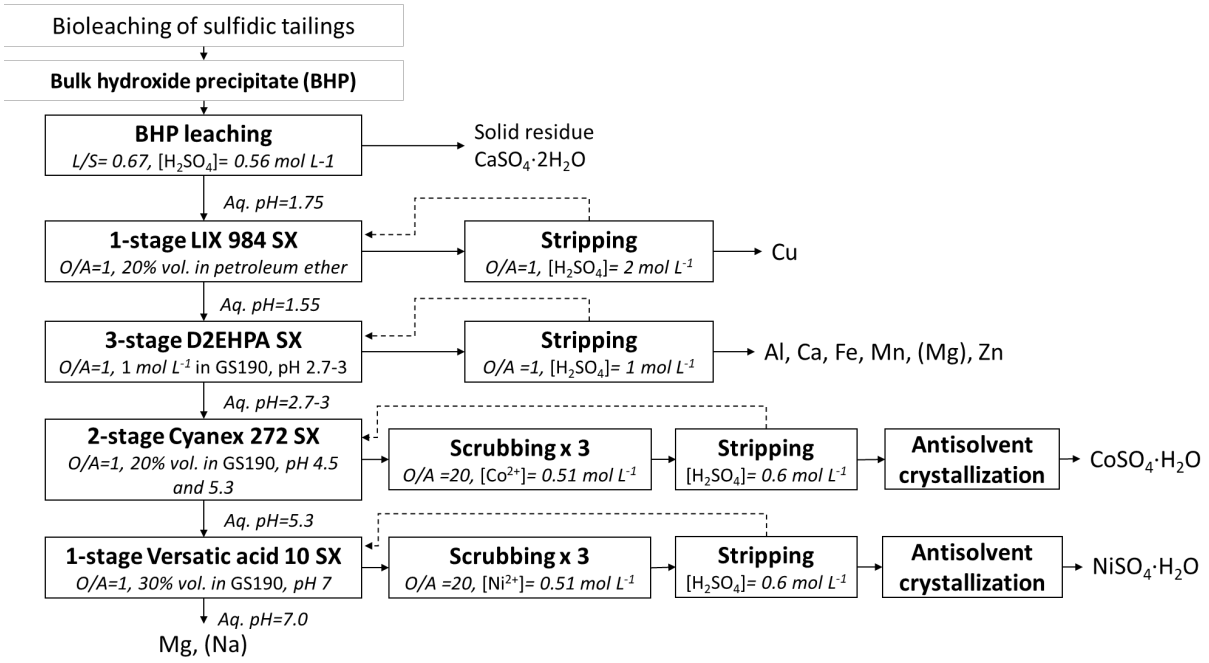

Figure 1: Conceptual flowsheet for production of cobalt and nickel sulfates from BHP obtained by bioleaching of sulfidic mine tailings.

This work's purpose was to test the technical feasibility of the conceptualized flowsheet. A detailed techno-economic assessment was outside the scope of this study. However, for sustainable and circular processes, the treatment of sulfate-bearing effluents, using the best available technologies (*i.e.* electrochemical salt splitting), should be considered in order to recover water, sulfuric acid, sodium hydroxide, and stabilize hazardous components.[33,34]

Besides, the current water balance, chemicals consumption, and production of secondary streams can be further improved and optimized.

3.2 BHP leaching

The BHP intermediate is a fine-grained powder obtained by precipitation of bioleached metals with commercial-grade lime, after the removal of iron and arsenic by precipitation. The chemical composition of the BHP is reported in Table 1. Small-scale tests were devised to optimize the leaching parameters and these tests showed that the sulfuric acid concentration was optimal between 0.5 and 1 mol L^{-1} at 25 °*C*, liquid-to-solid ratio L/S (L kg^{-1})= 10, 4 h (Figure 2 A). A sulfuric acid concentration of 1 mol L^{-1} was selected to study the other leaching parameters. Increasing the temperature accelerated the leaching processes and was associated with a slight decrease in magnesium and aluminum leachability (Figure 2 B, C, D) and an increase in that of manganese. More than 99.5% of cobalt, nickel, zinc, and copper were leached at any temperature and their leaching was the result of diffusion-controlled processes, as indicated by the kinetic study (Figure S5 and S6; Table S1) and the calculated activation energies ($Ea_{Cu, Zn, Co, Ni}$= 2.6–6.8 kJ mol^{-1}) below 20 kJ mol^{-1}.[35] In this work, the lower leaching temperature was selected to constrain the leaching of manganese, which is a potential interfering ion for metal purification by SX. Decreasing the L/S ratio from 10 to 5 did not affect the leaching of cobalt, nickel, zinc, and copper at equivalent boundary conditions ([H_2SO_4]= 1 mol L^{-1}; 25 °C; 4h) (Figure S7).

Optimization experiments performed on a 1 L scale led to a further decrease in sulfuric acid concentration, from 1 to 0.56 mol L^{-1}, using an operational L/S of about 6.7 (1 L/150 g) (Figure S8). When the BHP was leached in 0.56 mol L^{-1} sulfuric acid, the manganese and iron leaching efficiencies decreased. At the leaching pH≈ 1.8 with the lower sulfuric acid concentration, manganese and iron oxides (MnO_2 and Fe_2O_3) were thermodynamically more stable (Figure

S9) at the given leaching redox potentials (ORP > 1.1 V *vs* SHE) and temperature (35–45 °C) (Figure S10) than at pH 0.6 in 1 mol L^{-1} sulfuric acid leaching. The higher pH of the emerging PLS was also more adequate for the downstream metal separation by LIX 984 or D2EHPA.[36,37], reducing the acid consumption and the base needed for pH control during SX.

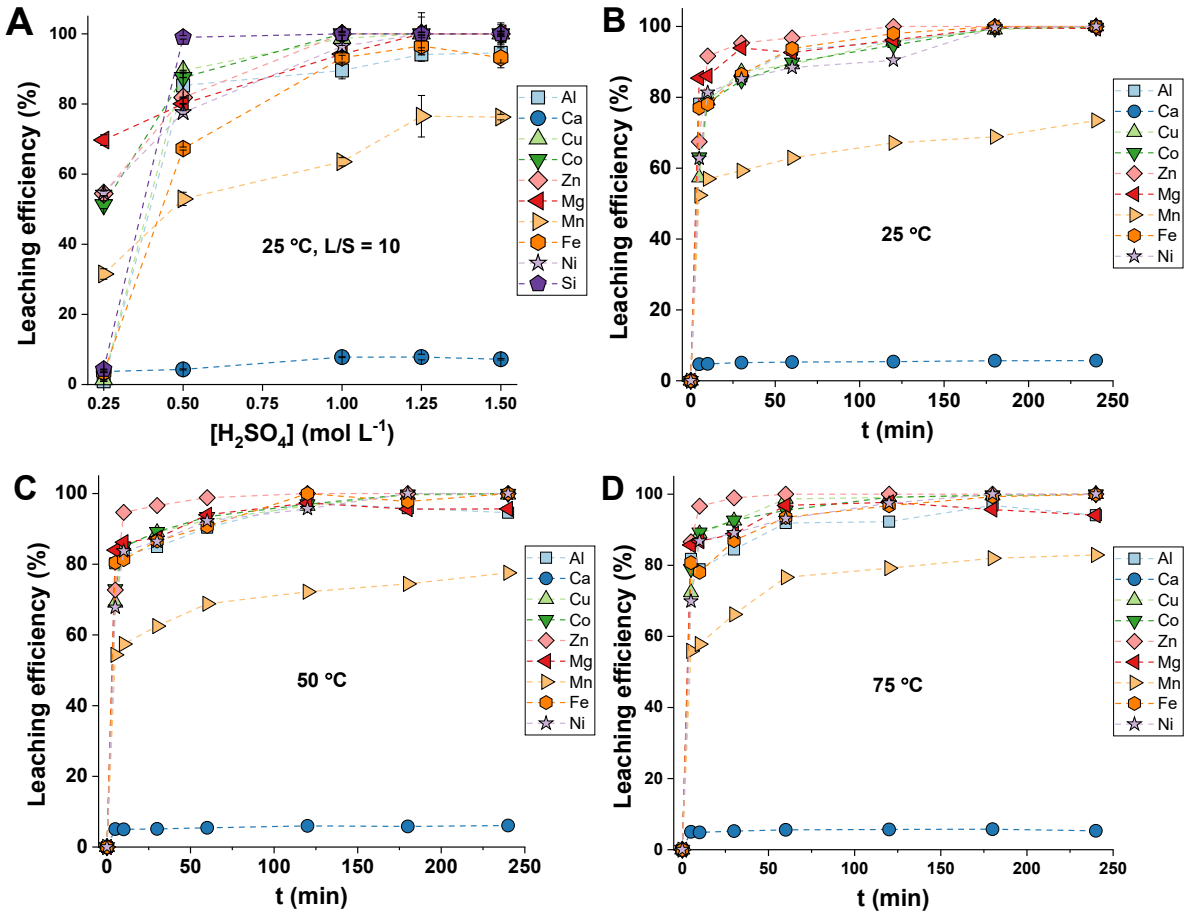

Figure 2: Effect of [H_2SO_4] ***(A)*** *and leaching temperature (25, 50, and 75 °C) for 4h, L/S= 10,* [H_2SO_4]= *1* mol L^{-1} ***(B)(C)(D)*** *on the leaching efficiencies of metals from BHP.*

To obtain suitable volumes of PLS for SX experiments, the optimal leaching conditions were reproduced in the 5 L scale reactor. Table 1 shows the PLS and the leach residue compositions that were used to define the mass balance for the BHP leaching. Comparable leaching efficiencies were observed in 1 L and 5 L reactors, as shown in Figure 3. Most of the leached metals could be recovered by washing the filter cakes under vacuum filtration, although minor metal concentrations were still observed in the leach residue. The stability of this residue should

be further investigated by standardized leaching tests to verify whether it can be safely disposed and/or reused.[38]

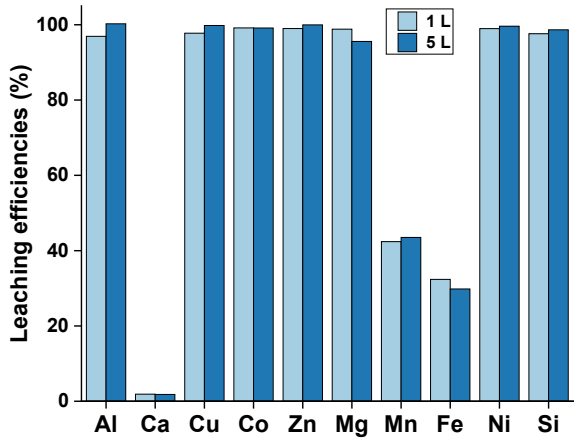

Figure 3: Leaching efficiencies (average from mass balances) in 1 L and 5 L reactors ($[H_2SO_4]$*= 0.56* mol L^{-1}*, 25 °C, L/S≈ 6.7, 3h).*

Table 1: Chemical compositions of BHP, PLS, and leach residue (5 L reactor, $[H_2SO_4]$*= 0.56* mol L^{-1}*, 25 °C, L/S≈ 6.7, 3*h*).*

Element	BHP (%)	PLS (mg L^{-1})	Residue (%)
Al	0.30±0.05	300±50	/
Ca	14±0.5	600±100	23±1
Cu	1.5±0.4	2000±150	0.011±0.001
Co	7.2±0.7	9500±1000	0.07±0.01
Zn	8.1±0.3	10000±1000	0.05±0.01
Mg	2.1±0.3	2500±500	/
Mn	1.0±0.1	900±100	0.9±0.1
Fe	0.10±0.01	30±1	0.02±0.01
Ni	4.2±0.4	5000±500	0.03±0.01
Si	0.60±0.01	750±20	/

Silicon was quantitatively leached from the BHP up to 750 ± 20 mg L^{-1}. It was verified that silicon was introduced as an impurity in the BHP with the lime precipitating agent. Colloidal

silica may affect SX circuits with severe operational problems, including crud formation, impurity transfer to the organic phase, poor phase disengagement, loss of chemicals, etc.[39,40]

At the obtained PLS pH, silicon is predominantly occurring as orthosilicic acid, $Si(OH)_4$.[41] Already in acidic media, orthosilicic acid undergoes ionization to $Si(OH)_3^-$ which results in the formation of Si oligomers $[SiO_x(OH)_{4-2x}]_n$ (where n = 2, 3), which can progressively grow as 3D Si-O-Si networks upon addition of monomers. Previous studies indicated that $Si(OH)_4$ ionization and polymerization are proportional to the pH increase.[42–44] At a suitable pH range for SX (3–7), dissolved silica may coalesce into gels or solid aggregates, affecting the SX operations. For these reasons, a silicon-free PLS is preferable, nevertheless, the dissolved silica behavior and its interaction with the SX systems were monitored along the flowsheet to identify the possible criticalities and mitigations.

3.3 LIX 984 SX: Cu recovery

Selective copper extraction is the most exploited technology to purify copper in the mining industry (leach–solvent extraction–electrowinning process, L-SX-EW), due to the tailored properties of the LIX 984 extractant and the advantage of acid regeneration in combination with electrowinning. Among the different selective copper extractants, LIX 984 is a mixture of *keto*- and *aldo*- oximes that provides a remarkable trade-off between copper extraction selectivity from other dissolved cations and the adequate coordination strength to facilitate the stripping of copper.[45] Hence, LIX 984 enabled selective copper extraction from the obtained PLS. A 20 vol% LIX 984 solution extracted 99.3% of copper in a single contact without pH adjustment of the PLS (Figure S11). ICP-OES analyses of the organic phase showed that no elements other than copper were co-extracted by the organic phase. Silicon was also stable in solution, without interfering with the LIX 984 organic phase (Figure S11).

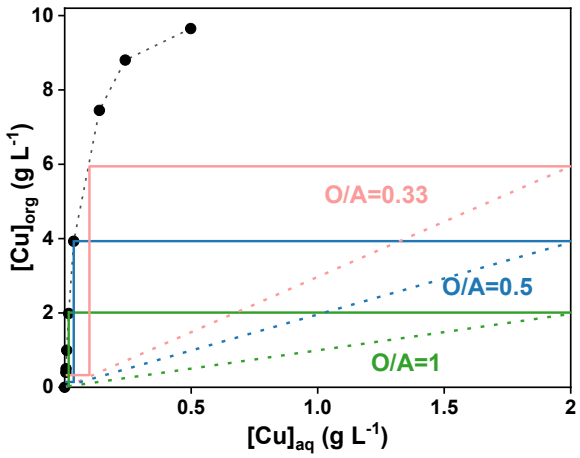

Figure 4: McCabe-Thiele diagram for Cu SX using LIX 984 20% vol. (non-saponified, room temperature, starting pH 1.74 ± 0.02, final pH 1.55± 0.03).

Lower concentrations of LIX 984 and/or O/A ratios can be used for real countercurrent application *i.e.* mixer-settlers in multiple-stage contacts, as also indicated by the McCabe-Thiele diagram (Figure 4) constructed using 20 vol% LIX at various O/A. A single contact at O/A= 0.5 might be sufficient to remove more than 95% of the Cu and the number of stages to achieve quantitative extraction could be either 2 to 3 depending on the O/A ratio. However, for this study, a single step with 20 vol% LIX was deemed acceptable to further investigate the Zn and other impurities extraction from the copper-depleted PLS.

This approach solved any potential loss of copper due to the co-extraction in D2EHPA and Cyanex 272, leaving in the raffinate 10±5 mg L^{-1} of copper (Table S2). Instead, when a three-stage countercurrent simulation with D2EHPA was tested on the PLS, copper was not quantitatively extracted, yielding about 85%, along with zinc and other impurities (Figure S12). Therefore, it also simplifies the copper recovery compared to the recovery from the D2EHPA stripping solution containing many other elements. Additionally, about 15% of copper would follow to the next Cyanex 272 SX stage as an interfering ion.

LIX 984 extraction was validated in batch mode on a 1 L scale for an extraction-stripping-extraction cycle. The first extraction selectively extracted 99.3% copper selective extraction.

About 96% of copper was recovered following a stripping step with a 2 mol L^{-1} sulfuric acid solution (A/O= 1). The second extraction with the regenerated organic phase achieved 99.1% of copper extraction. In the conditions studied, the LIX 984 organic phase is not saturated with copper. Conversely, copper buildup in the organic phase is common for oxime-based extractants, due to the strong coordination. The copper that cannot be stripped reaches a constant concentration in the organic phase during continuous SX, decreasing the overall extraction capacity of the system, which is taken into account in the SX-EW copper refining processes. As a rule of thumb for each g L^{-1} of copper in the PLS, 4 vol. % of extractant in diluent is considered to guarantee that the organic phases containing copper can be industrially recirculated in continuous SX circuits.[45]

The copper concentration in the BHP PLS ($[Cu^{2+}]$= 2 g L^{-1}) falls within the conventional PLS concentration range of copper mining (1–10 g L^{-1}) that undergoes SX for selective copper extraction. In industry, copper is then up-concentrated in the SX-EW circuits, performing the stripping with the spent electrolyte ≈ 35 g L^{-1} to a suitable concentration for EW ≈ 45 g L^{-1}.[45] Therefore, it might be assumed that copper could be selectively recovered from the BHP PLS by a SX-EW process.

3.4 D2EHPA SX: zinc and impurity removal

After LIX 984 SX, the aqueous raffinate still contains nine major elements (Table 1). Purification with D2EHPA is a crucial operation to ensure acceptable conditions for cobalt-nickel separation by removing troublesome interfering elements (Al, Ca, Cu, Zn, Fe, Mn, and Mg) that would eventually be co-extracted by Cyanex 272. Preliminary optimization of the system (Figure S13,14) indicated that a D2EHPA concentration of 1 mol L^{-1} (≈33.6 vol%) and an O/A ratio of 1 maximize the removal of impurities while improving the separation factors (Table S3) against cobalt and nickel at pH values between 2.7 and 3.0. These results also

showed the expected extraction order (Fe > Zn > Al > Ca > Mn > Cu >> Mg, Co, Ni) as a function of increasing pH.[32]

Aluminum, calcium, iron, and zinc were quantitatively extracted from the PLS. As distribution ratios for manganese and copper were low ($5 < D_{Mn} < 10$; $1.5 < D_{Cu} < 3.5$), their repartition between the aqueous and organic phase in countercurrent was difficult to predict, due to the possible competing effect over multiple SX stages. As soon as saturated D2EHPA is re-contacted with fresh aqueous solutions, metal cations exhibiting higher coordination strength with D2EHPA may induce the stripping of less strongly coordinated cations to the aqueous phase. Therefore, rather than the conventional McCabe-Thiele diagram, a batch simulation was performed to obtain a more realistic description of the behavior of the different metals in countercurrent mode.

Controlling and adjusting the pH to 2.7–3.0 in every batch experiment for all three stages was ensuring acceptable metal impurity removal rates and limited cobalt losses. Pre-saponification of the D2EHPA organic phase was used to control the pH. Silicon concentration in the aqueous solution was unaffected during the entire simulation using the saponified D2EHPA organic phase.

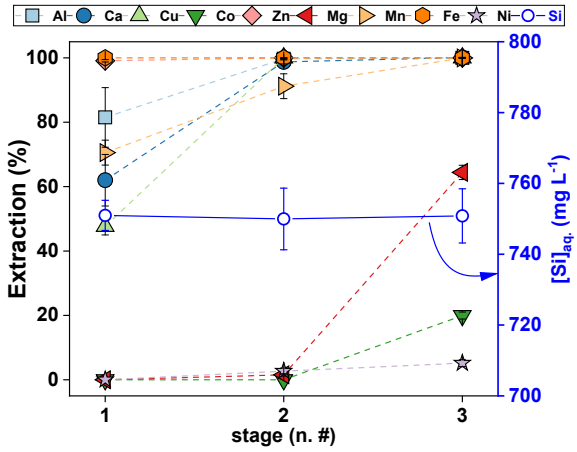

Figure 5: Three-stage countercurrent simulation at pH 2.7–3.0 ([D2EHPA]= 1 mol L^{-1} (≈ 33.6 vol%), *40–45% saponification, O/A= 1, room temperature).*

With three countercurrent stages, the quantitative removal of aluminum, calcium, copper, zinc, iron, and manganese was achieved (Figure 5). In the third stage, the magnesium extraction (64±2%) was significantly higher than the extraction of cobalt (20±1%) and nickel (5±1%). This is beneficial for the next SX process with Cyanex 272 which suffers from poor efficiency in cobalt-magnesium separation. Cobalt and magnesium extraction curves *vs* pH show only a narrow $\Delta pH_{1/2}$ for separation or even intersection, depending on the relative concentrations of metals and extractant.[32,46] In favor of a more purified solution for the Cyanex 272 stage, a cobalt loss of 20% was accepted. Decreasing the pH in the 1st stage might strip cobalt, enhancing cobalt recoveries. Alternatively, a two-stage countercurrent significantly minimizes the cobalt loss during D2EHPA SX, although it might result in more intricate Mg-Co separation, to scrub higher concentrations of Mg from Cyanex 272. All the calculated metal extractions are reported in Table S4.

Explorative stripping tests of zinc and impurities showed that most of the extracted metals can be released from the organic phase (1-stage) via a single contact with a 1 mol L^{-1} sulfuric acid solution at a phase ratio O/A= 1 (Figure S16), besides the stripping of aluminum that was only taking place at a sulfuric acid concentration of 3 mol L^{-1}. At this concentration, precipitation started to occur and became quite extensive at concentrations of 4 mol L^{-1} reaching the saturation limits for Al and Ca sulfates.

Further research should be addressed to the optimization of the stripping, and recovery of zinc and other metals, as well as to the reuse of the metal-depleted stripping solution. Zinc can provide interesting economic revenue. Selective precipitation as ZnS might be a valuable approach.[47,48]

3.5 Cyanex 272 SX: cobalt-nickel separation

Cyanex 272 SX offers the property to extract cobalt as a tetrahedral complex in the organic phase selectively from nickel that prefers octahedral coordination.[49] The previous SX with D2EHPA removed some troublesome metal cations for the cobalt-nickel separation (Zn, Ca, Cu, Mn, etc.). However, magnesium and silicon persisted in the purified raffinate which may have undesirable effects on the cobalt-nickel separation.

Figure 6 A presents the extraction efficiencies as a function of the volumetric concentrations of Cyanex 272, saponified as 55% of its molar concentration ([NaOH] = 0.55 [Cyanex 272]). Cobalt extraction increased with Cyanex 272 concentration but so did the extraction of magnesium and nickel. It should be noted that also the equilibrium pH varied with the Cyanex 272 concentration in these experiments.

A 20 vol% concentration guaranteed limited co-extraction of magnesium and nickel, and silicon precipitation. This concentration also gave a more stable organic phase in countercurrent simulation than 10 vol%, whereby the organic phase aggregated at high cobalt loads (Figure S17). The effect of equilibrium pH, at this extractant concentration, showed that about 70% of cobalt was selectively extracted at 4.5 equilibrium pH (Figure 6 B). Moreover, silicon losses due to the transfer to the organic phase and silicon-bearing precipitates in the aqueous phase (Figure S17) were relatively low. Decreasing the saponification degree of Cyanex 272 to 30% enabled obtaining an equilibrium pH of 4.5 and avoided silicon precipitation and crud formation.

For the batch countercurrent simulation, a two-stage process at two distinct pH values of 4.5 and 5.3, respectively, was optimized. A lower pH in the first SX stage gave good scrubbing of impurities (Mg, Ni) from the output organic phase. However, an equilibrium pH> 5 in the second SX stage was required to maximize the cobalt recovery.[50], although co-extraction of magnesium and nickel occurred.

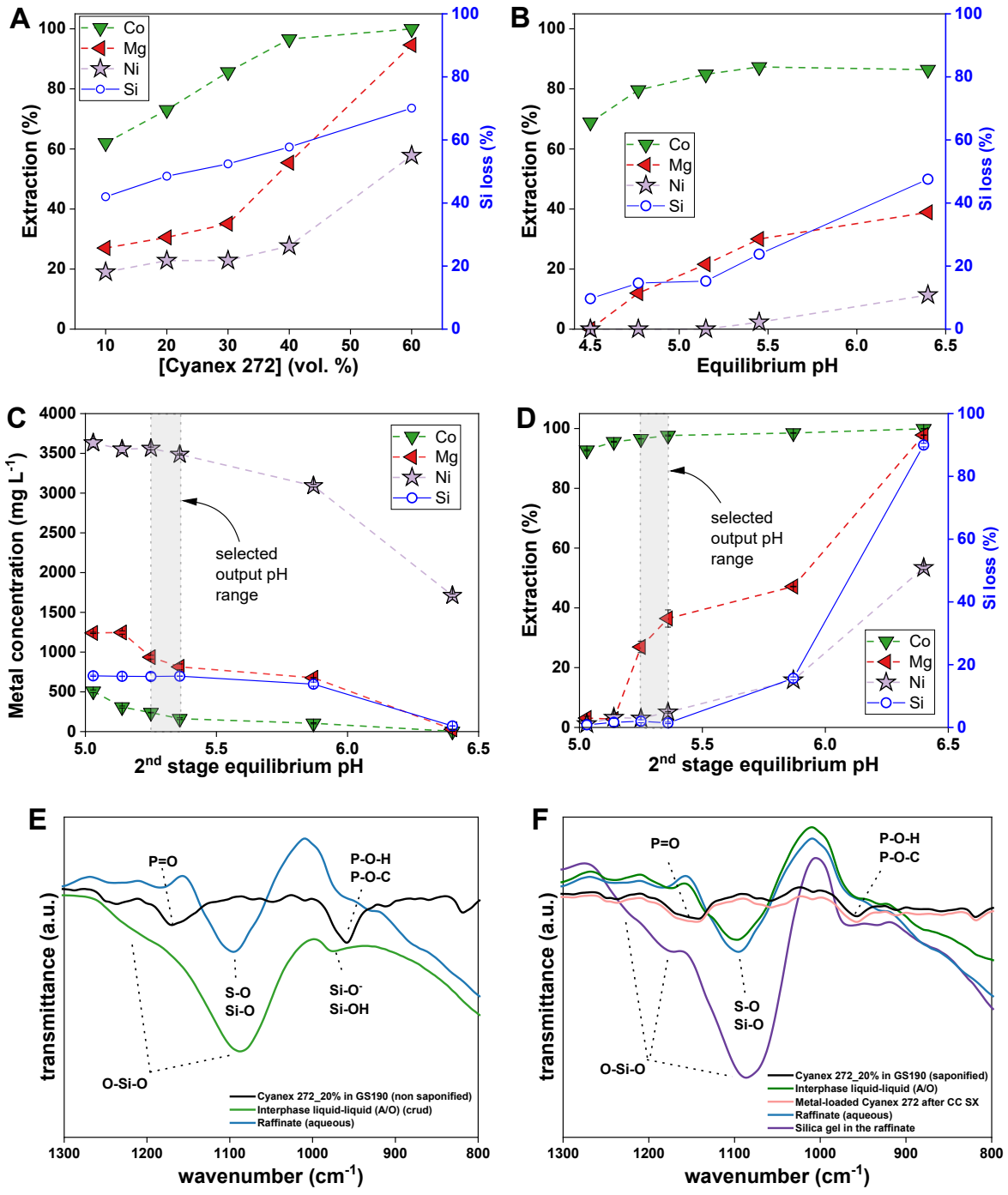

Figure 6: ***(A)*** *Metal extraction curves from D2EHPA countercurrent simulation raffinate as a function of Cyanex 272 concentration (vol%.), 55% saponification* ***(B)*** *and as a function of the equilibrium pH (20 vol% Cyanex 272, 30% saponification), O/A= 1, room temperature.* ***(C)*** *Metal concentration profile in the raffinate by two-stage Cyanex 272 countercurrent simulation and* ***(D)*** *metal extraction curves by a two-stage Cyanex 272 countercurrent simulation as a function of the 2nd stage equilibrium pH (20 vol% Cyanex 272, 30% saponification, O/A= 1, room temperature). FTIR spectra of the non-saponified Cyanex 272 SX system, whereby dissolved silica was involved in crud and precipitate*

*formation **(E)** and saponified Cyanex 272 system, whereby dissolved silica was only involved in the formation of silica gel in the aqueous raffinate overtime after countercurrent SX **(F).***

Hence, the equilibrium pH in the second stage determines the impurity co-extraction as well as the cobalt extraction efficiency, at given metal concentrations. Additionally, this pH value also influences the stability of the dissolved silica in the aqueous solution. Therefore, the equilibrium pH of the second stage was investigated, as in Figure 6 C and D, and an optimal equilibrium pH was about 5.3. With this pH, the overall metal extraction to the organic phase yielded 97, 32, and 4% for cobalt, magnesium, and nickel respectively, without appreciable silicon losses throughout the simulation nor transfer to the organic phase.

Comparison of the FTIR spectra in the mid-IR region 1300-800 cm^{-1} (diagnostic for the silica-bearing solutions, gels, and solids),[51,52] of the non-saponified versus the saponified Cyanex 272 SX systems (Figure 6 E, F) showed that colloidal silica had been formed at the liquid-liquid interphase in the non-saponified system, upon direct addition of NaOH solution to adjust the equilibrium pH, resulting in crud formation. On the other hand, colloidal silica was not observed at the liquid-liquid interphase in the saponified system during the entire countercurrent simulation. Thus, crud formation as well as precipitate formation in the non-saponified SX system was associated with the local interaction of Si-O-Si polymeric precursors with hydroxide anions of the base. FTIR spectra for the liquid-liquid interphase in the presence of crud (Figure 6 E) showed a more intense absorption band at about 974 cm^{-1} compared with the silica-bearing precipitate (Figure S17) and silica gel formed in the raffinate after countercurrent extraction over time (Figure 6 F). Such a band is consistent with the stretching vibrations of Si-OH and/or $Si\text{-}O^-$ groups on the surface.[52–54] The interaction of silica gel with non-polar solvent is proportional with the number of silanol groups responsible for hydrogen bonds and the adsorption of organic molecules onto the silica gel,[55] which, in turn, may determine the crud formation. Furthermore, FTIR spectra of the silica-bearing precipitate and gel in the SX

raffinate (Figure S18) showed more pronounced shoulders at about 1220, 1175, and 1130 cm^{-1} to the main peak at 1085 cm^{-1}, corresponding to Si-O-Si stretching vibrations, suggesting a higher degree of condensation into larger polymeric structures than those participating in the crud formation. Thus, larger agglomerates presenting fewer surface charge/silanol groups settle at the bottom of the aqueous phase either as solids or sol-gels[51,55].

As shown in Figure 6 F, despite the silicon concentration being unvaried in the solution (Table S5), the formation of a gel was observed in the nickel-rich raffinate (Figure S17) associated with the silica polymerization and gelation process at increasing pH.[56]

The silica gelation process is also influenced by the presence of alkali and alkaline-earth cations in solutions. Sodium ions (Na^+) that are exchanged from the saponified organic to the aqueous phase are known to decelerate slow down the condensation reaction of hydrated monomers, and oligomers.[57] Furthermore, sodium ions may weaken the Si-O-Si, stabilizing hydrated silica monomers (Na-O-$Si(OH)_3$), which may be released in solution from dimers/oligomers.[57] Literature studies indicate that the colloidal silica gelation rate (t_{gel}) is inversely correlated with the Hofmeister series and the characteristic hydration diameter of the dissolved cations. Therefore, in the presence of sodium, the formation of silica gel is a slower process.[58,59] In the countercurrent SX extraction conditions, the silica gelation solely occurred in the raffinate over days, thus, it is assumed that Cyanex 272 SX could be performed in continuous mode, although dedicated experimentation in mixer-settlers should corroborate the results obtained here. The aqueous raffinate, yet, is not sufficiently stable to perform nickel-magnesium separation in the next Versatic Acid 10 SX circuit, taking place at an even higher pH.[60]

For cobalt recovery, the scrubbing of the cobalt-loaded organic phase was necessary to remove the co-extracted nickel, magnesium, and sodium. This latter was not completely released in the aqueous solution during SX and remained, to a little extent, in the organic phase from the

extractant's saponification. Preferential extraction of cobalt over magnesium, nickel and sodium can be exploited to further purify the cobalt-loaded organic phase. Essentially, cobalt cations are exchanged for magnesium, nickel and sodium during scrubbing. The latter are released back to the contacted aqueous phase. Increasing the number of scrubbing stages evidenced the gradual removal of the abovementioned elements from the organic phase (Figure 7 A).

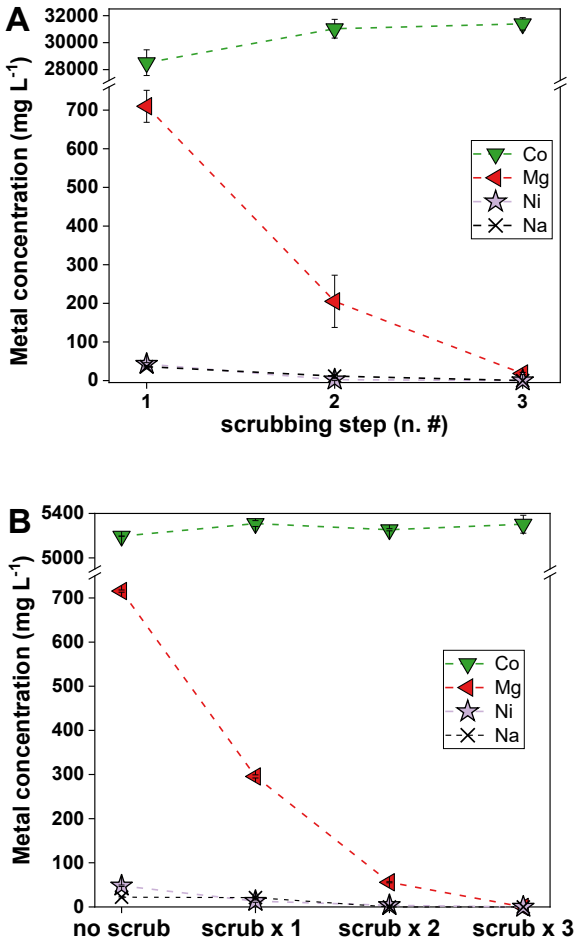

Figure 7: ***(A)*** *Metal concentration profile in the aqueous scrubbing solutions in crosscurrent (*$[Co^{2+}]$*= 0.5* mol L^{-1}*, O/A= 20, room temperature) as a function of scrubbing steps.* ***(B)*** *Metal concentration profile in the aqueous stripping solutions (*$[H_2SO_4]$*= 0.6* mol L^{-1}*, O/A= 1, room temperature) as a function of scrubbing steps.*

Three scrubbing stages were considered sufficient to achieve acceptable cobalt product purity from the emerging stripping solution, whereby no nickel, magnesium, or sodium was detected in addition to about 30 g L^{-1} of cobalt (Figure 7 B). Cobalt stripping was achieved in a single contact with a sulfuric acid solution equal to or larger than 0.6 mol L^{-1}.

3.6 Versatic Acid 10 SX: nickel-magnesium separation

The gel formation after Cyanex 272 SX countercurrent simulation is a showstopper for SX, especially in continuous mode. Versatic Acid 10 SX experiments at pH> 5.5 on the fresh raffinate solution, before gel formation, led to a further precipitation of silica-bearing solids in the aqueous solution, also after saponification of the extractant (Figure S19).

Nevertheless, the nickel extraction was investigated on the filtered solutions as a proof-of-principle for testing the flowsheet's feasibility in a silicon-free scenario. The concentration of silicon was <1 mg L^{-1} after filtration with a 0.45 μm porous media,[40] indicating that the dissolved silica and its aggregation/condensation were responsible for crud and precipitate formation. Membrane filtration might be an expensive and time-consuming solution for industrial-relevant flowsheets, with unwanted losses of nickel (and extractant/diluent) in the silica gel (Figure S18).

The effect of the equilibrium pH at a constant concentration of Versatic Acid 10 in GS190 diluent (40 vol%) showed that the optimal pH for quantitative extraction of nickel was about 7 (Figure 8A), as indicated by the composition of the aqueous solutions before after extraction (Table S6). A 20 vol% concentration gave 99.5% nickel extraction, at comparable nickel concentrations, to increase further to 99.9% at 30 vol%, working at an equilibrium pH of 7.0± 0.2 (Figure 8B).

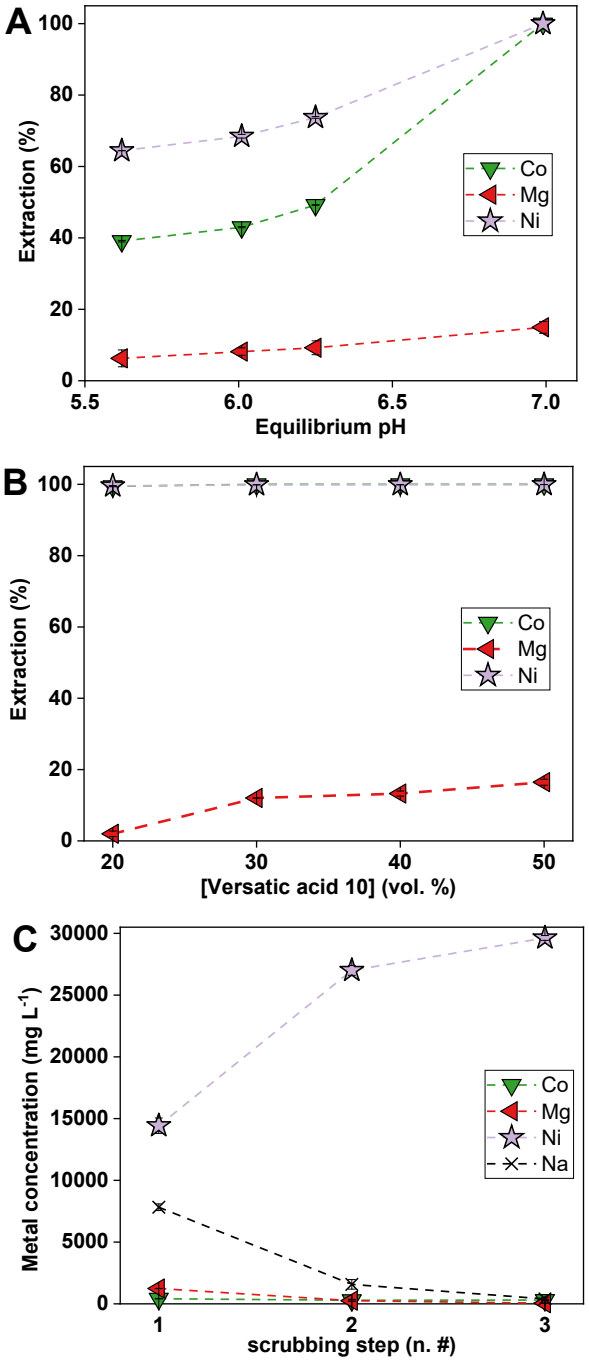

Figure 8: ***(A)*** *Metal extraction curves as a function of the equilibrium pH for Versatic Acid 10 (40 vol% in GS190, O/A= 1 and* ***(B)*** *as a function of the Versatic Acid 10 concentration (vol%) in GS190, (O/A = 1, pH 7.0±0.2), room temperature.* ***(C)*** *Metal concentration profile in the scrubbing solutions (*$[Ni^{2+}]$*= 0.5* mol L^{-1}*, O/A= 20) as a function of the scrubbing steps in crosscurrent.*

This latter condition was selected for nickel recovery, although co-extraction of cobalt (100%) and magnesium (12%) took place. Therefore, scrubbing was employed to remove the unwanted metals (magnesium, cobalt, and sodium). Three stages were investigated to scrub these impurities before the crystallization of the final product. Figure 8 C shows that the Versatic Acid 10 organic phase is far from the saturation in the first two scrubbing steps, whereas working close to saturation can decrease the impurity transfer to the organic phase and decrease the number of scrubbing steps.

3.7 Antisolvent crystallization of $CoSO_4 \cdot H_2O$ and $NiSO_4 \cdot H_2O$

The predominant cobalt- and nickel-based battery precursors on the market are the heptahydrate and hexahydrate forms, respectively. Recent studies indicated that dedicated crystallization set-ups (*i.e.* pressure crystallizers, continuous crystallizers), in-depth optimization of the crystallization (*i.e.* crystallization temperature, evaporation flux, time, seeding) and post-crystallization parameters (*i.e.* cooling, drying temperature, and time) would be needed to stabilize the sulfates in the above-mentioned structures, which are also affected by the presence of impurities.[61–63] In this work, a fast crystallization procedure was applied to obtain nickel and cobalt sulfates, aiming at a single polymorph with stable water content/hydration, enabling to define of solids' purity, as an indicator of the performances of the applied flowsheet for battery-metal separation from the BHP.

An arbitrary excess of acetone (O/A= 6) was used to ensure the quantitative precipitation of cobalt and nickel. Applying ultrasounds for 30 s was sufficient to induce the instantaneous precipitation of the metal sulfates with negligible evaporation of the water-acetone system in the closed vials [30]. Acquired XRD patterns defined that a main phase of $CoSO_4 \cdot H_2O$ (COD 9009371, monoclinic) composed the products after drying at 60 °C, even without scrubbing (Figure S20). Furthermore, the XRD of the purchased $CoSO_4 \cdot 7H_2O$ after dehydration at 60 °C matched with the patterns of the $CoSO_4 \cdot H_2O$ recovered from the BHP purification (Figure 9A).

The $CoSO_4 \cdot H_2O$ purity increased progressively with the number of scrubbing steps, until reaching 99.5% after three scrubbing steps.

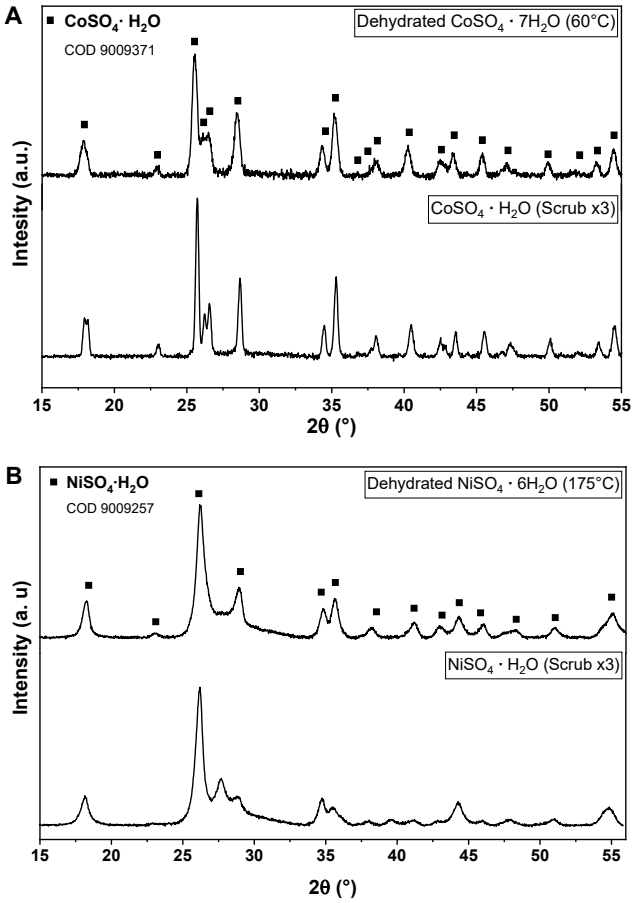

Figure 9: XRD of the $CoSO_4 \cdot H_2O$ *(3× scrub) obtained from the BHP compared with the dehydrated* $CoSO_4 \cdot 7H_2O$ *at 60* °C **(A)** *and XRD of the* $NiSO_4 \cdot H_2O$ *(3× scrub) obtained from the BHP compared with the dehydrated* $NiSO_4 \cdot 7H_2O$ *at 175* °C **(B)**.

The XRD study on the obtained nickel(II) sulfate products demonstrated a main phase of $NiSO_4 \cdot H_2O$ (COD 9009257, monoclinic) in agreement with the most stable nickel(II) sulfate phase at 175 °C.[64] Without scrubbing, the nickel sulfate product showed a less crystalline structure (Figure S21) in combination with a lower purity (≈90%, Table 2) due to cobalt, magnesium, and sodium impurities. The metal compositions of the obtained cobalt and nickel sulfates can be found in Table S7.

When comparing the XRD patterns of the obtained product after 3 scrubbing stages with the purchased $NiSO_4 \cdot 6H_2O$ dehydrated at 175 °C (Figure 9B), the presence of a secondary monoclinic structure of the group C 1 2/C 1 (15) was observed, which is associated with the occurrence of cobalt as $CoSO_4 \cdot H_2O$.

Table 2: Purity of $CoSO_4 \cdot H_2O$ and $NiSO_4 \cdot H_2O$ obtained after SX metal separations and antisolvent crystallization

$CoSO_4 \cdot H_2O$	**Purity(%)**
No scrub	95.8±0.6
2 × scrub	97.7±0.7
3 × scrub	99.5±0.5
$NiSO_4 \cdot H_2O$	**Purity(%)**
No scrub	90.9±0.1
3 × scrub	98.8±0.2

It should be mentioned that the raffinate used for recovering nickel products was coming from a countercurrent simulation with Cyanex 272 at an equilibrium output pH of 5.0, which exhibited higher cobalt content (500 mg L^{-1}, Table S6) than the raffinate produced at pH 5.3 (250 mg L^{-1}, Table S5). Cobalt was co-extracted with nickel by Versatic Acid 10 with a negative effect on the purity of the final nickel product. This suggests that the cobalt content in the nickel product could be decreased further by optimizing upstream conditions. Furthermore, a 2-stage countercurrent process with Versatic Acid 10 may provide a more efficient scrubbing of the impurities for the exiting nickel-loaded organic phase, before the organic phase undergoes scrubbing.

This part of the study indicated that battery-grade sulfates might be obtained from the studied BHP using the proposed flowsheet, by carefully controlling and optimizing the crystallization conditions and/or by crystallizing the solids directly from the stripping solutions with the best available techniques (Ma et al., 2020).

4. Conclusions

The present work demonstrates the technical feasibility of an SX-based flowsheet to obtain pure cobalt(II) and nickel(II) sulfates from a complex BHP produced by bioleaching of metals from sulfidic mine tailings.

The main conclusions may be summarized as follows:

1) LIX 984 SX selectively separated 99% of copper, indicating a valuable solution for copper recovery in SX-EW circuits.
2) A three-step countercurrent simulation of the SX with D2EHPA removed 100% of the aluminum, calcium, iron, and manganese and 60% of magnesium at pH 2.7–3.0. 20% of cobalt was also coextracted.
3) A two-step countercurrent simulation of the SX with Cyanex 272 at pH achieved 97% of cobalt separation and recovery in the D2EHPA raffinate (77% of the total). A pure cobalt sulfate stripping solution was obtained after three scrubbing steps.
4) Versatic Acid 10 SX could separate nickel from magnesium at pH 7 only after filtration and removal of the silica gel that forms in the Cyanex 272 raffinate over days. Scrubbing enhanced the purity of the nickel sulfate stripping solution.
5) Ultrasound-assisted antisolvent crystallization may be employed to recover pure cobalt and nickel sulfates efficiently.
6) Dissolved silica in the PLS is a serious concern in the implementation of SX. Crud formation was avoided by the saponification of D2EHPA and Cyanex 272 organic phases. Preventing the direct interaction of O-Si-O precursors in solution with hydroxyl anions, generating silica networks exhibiting surface $Si\text{-}O^-$ and Si-OH groups, suppress the organic solvents' adsorption, hindering the silica stabilizing at the liquid-liquid interphase forming the crud. Whereas, gels and or precipitates showed minor surface groups and higher degree of polymerization of the Si–O–Si structures.

Supporting Information

Supporting information contains a description of SX simulations; the kinetic study, in-depth study of leaching parameters (L/S, kinetic study, ORP and pH profiles for leaching in 1 L and 5 L leaching, Mn and Fe Pourbaix diagrams); supplementary information for the D2EHPA, Cyanex 272, and Versatic Acid 10 SX systems (pictures, separation factors, FTIR spectra, silica gel characterization); supplementary XRDs and chemical composition of the aqueous streams.

Acknowledgments

This study received funding under the EU Framework Programme for Research and Innovation Horizon 2020, NEMO project Grant Agreement No 776846. This work reflects the author's view and the Agency is not responsible for any use that may be made of the information it contains.

Boliden Mineral AB (Sweden) is acknowledged for kindly providing the BHP as starting material for this experimentation. Special thanks to Anders Sand, Mohammad Khoshkhoo, and Caroline Kihlblom from the R&D department of Boliden Mineral AB for the fruitful collaboration.

Conflict of interest

There are no conflicts to declare.

References

(1) Buchholz, P.; Brandenburg, T. Demand, Supply, and Price Trends for Mineral Raw Materials Relevant to the Renewable Energy Transition Wind Energy, Solar Photovoltaic Energy, and Energy Storage. *Chemie-Ingenieur-Technik* **2018**, *90* (1), 141–153. https://doi.org/10.1002/cite.201700098.

(2) Månberger, A.; Johansson, B. The Geopolitics of Metals and Metalloids Used for the Renewable Energy Transition. *Energy Strateg. Rev.* **2019**, *26* (July), 100394. https://doi.org/10.1016/j.esr.2019.100394.

(3) Gregoir, L.; van Acker, K.; Beretta, S.; Heron, C. *Metals for Clean Energy : Policymaker Summary*; 2022. https://eurometaux.eu/media/20ad5yza/2022-policymaker-summary-report-final.pdf.

(4) Hagelüken, C.; Goldmann, D. Recycling and Circular Economy—towards a Closed Loop for Metals in Emerging Clean Technologies. *Miner. Econ.* **2022**, *35* (3–4), 539–562. https://doi.org/10.1007/s13563-022-00319-1.

(5) Lèbre, É.; Stringer, M.; Svobodova, K.; Owen, J. R.; Kemp, D.; Côte, C.; Arratia-Solar, A.; Valenta, R. K. The Social and Environmental Complexities of Extracting Energy Transition Metals. *Nat. Commun.* **2020**, *11* (1), 1–8. https://doi.org/10.1038/s41467-020-18661-9.

(6) Akcil, A.; Koldas, S. Acid Mine Drainage (AMD): Causes , Treatment and Case Studies. **2006**, *14*, 1139–1145. https://doi.org/10.1016/j.jclepro.2004.09.006.

(7) Venkateswarlu, K.; Nirola, R.; Kuppusamy, S.; Thavamani, P.; Naidu, R.; Megharaj, M. Abandoned Metalliferous Mines: Ecological Impacts and Potential Approaches for Reclamation. *Rev. Environ. Sci. Biotechnol.* **2016**, *15* (2), 327–354. https://doi.org/10.1007/s11157-016-9398-6.

(15) Cao, J.; Zhang, G.; Mao, Z.; Fang, Z.; Yang, C. Precipitation of Valuable Metals from Bioleaching Solution by Biogenic Sulfides. *Miner. Eng.* **2009**, *22* (3), 289–295. https://doi.org/10.1016/j.mineng.2008.08.006.

(16) Williams, C.; Hawker, W.; Vaughan, J. W. Selective Leaching of Nickel from Mixed Nickel Cobalt Hydroxide Precipitate. *Hydrometallurgy* **2013**, *138*, 84–92. https://doi.org/10.1016/j.hydromet.2013.05.015.

(17) Chen, G.; Yang, H.; Li, H.; Tong, L. Recovery of Cobalt as Cobalt Oxalate from Cobalt Tailings Using Moderately Thermophilic Bioleaching Technology and Selective Sequential Extraction. *Minerals* **2016**, *6*, *67* (3), 6030067. https://doi.org/10.3390/min6030067.

(18) Ichlas, Z. T.; Mubarok, M. Z.; Magnalita, A.; Vaughan, J.; Sugiarto, A. T. Processing Mixed Nickel-cobalt Hydroxide Precipitate by Sulfuric Acid Leaching Followed by Selective Oxidative Precipitation of Cobalt and Manganese. *Hydrometallurgy* **2020**, *191* (November 2019), 105185. https://doi.org/10.1016/j.hydromet.2019.105185.

(19) Flett, D. S. Cobalt-Nickel Separation in Hydrometallurgy: A Review. *Chem. Sustain. Dev.* **2004**, *12*, 81–91.

(20) Flett, D. S. Solvent Extraction in Hydrometallurgy: The Role of Organophosphorus Extractants. *J. Organomet. Chem.* **2005**, *690* (10), 2426–2438. https://doi.org/10.1016/j.jorganchem.2004.11.037.

(21) Wilson, A. M.; Bailey, P. J.; Tasker, P. A.; Turkington, J. R.; Grant, R. A.; Love, J. B. Solvent Extraction: The Coordination Chemistry behind Extractive Metallurgy. *Chem. Soc. Rev.* **2014**, *43* (1), 123–134. https://doi.org/10.1039/c3cs60275c.

(22) Hu, F.; Wilson, B. P.; Han, B.; Zhang, J.; Louhi-Kultanen, M.; Lundström, M. High

Purity Nickel Recovery from an Industrial Sidestream Using Concentration and Liquid–Liquid Extraction Techniques. *JOM* **2020**, *72* (2), 831–838. https://doi.org/10.1007/s11837-019-03928-4.

(23) Guimarães, A. S.; Da Silva, P. S.; Mansur, M. B. Purification of Nickel from Multicomponent Aqueous Sulfuric Solutions by Synergistic Solvent Extraction Using Cyanex 272 and Versatic 10. *Hydrometallurgy* **2014**, *150*, 173–177. https://doi.org/10.1016/j.hydromet.2014.10.005.

(24) Estay, H.; Barros, L.; Troncoso, E. Metal Sulfide Precipitation: Recent Breakthroughs and Future Outlooks. *Minerals* **2021**, *11* (12), 1–27. https://doi.org/10.3390/min11121385.

(25) Soeezi, A.; Haghshenas-Kashani, B.; Farahmand, F.; Osanloo, A. Extraction of Co, Ni and Cu by the Solvent Extraction Method with Simulation Setup for Control, Alarm and Protection System. *Can. Metall. Q.* **2022**, *61* (1), 33–47. https://doi.org/10.1080/00084433.2022.2027079.

(26) Akbari, S.; Ahmadi, A. Recovery of Copper from a Mixture of Printed Circuit Boards (PCBs) and Sulphidic Tailings Using Bioleaching and Solvent Extraction Processes. *Chem. Eng. Process. - Process Intensif.* **2019**, *142* (June), 107584. https://doi.org/10.1016/j.cep.2019.107584.

(27) Dash, S.; Mohanty, S. Mathematical Modeling Aspect in Solvent Extraction of Metals. *Sep. Purif. Rev.* **2021**, *50* (1), 74–95. https://doi.org/10.1080/15422119.2019.1648294.

(28) Moyer, B. A., *Ion Exchange and Solvent Extraction: Changing the Landscape in Solvent Extraction*; CRC Press, Roca Baton, **2019**, Volume 23, 1–311. https://doi.org/10.1201/9781315114378.

(29) Omelchuk, K.; Stambouli, M.; Chagnes, A. Investigation of Aggregation and Acid Dissociation of New Cationic Exchangers for Liquid-Liquid Extraction. *J. Mol. Liq.* **2018**, *262*, 111–118. https://doi.org/10.1016/j.molliq.2018.04.082.

(30) Jia, S.; Yang, P.; Gao, Z.; Li, Z.; Fang, C.; Gong, J. Recent Progress in Antisolvent Crystallization. *CrystEngComm* **2022**, *24* (17), 3122–3135. https://doi.org/10.1039/d2ce00059h.

(31) Alvial-Hein, G.; Mahandra, H.; Ghahreman, A. Separation and Recovery of Cobalt and Nickel from End of Life Products via Solvent Extraction Technique: A Review. *J. Clean. Prod.* **2021**, *297*, 126592. https://doi.org/10.1016/j.jclepro.2021.126592.

(32) Sole, K. C. Solvent Extraction in the Hydrometallurgical Processing and Purification of Metals Process Design and Selected Applications. In *Solvent Extraction and Liquid Membranes: Fundamentals and Applications in New Materials*; CRC press, Boca Raton, 2008, 141–200. https://doi.org/10.1201/9781420014112.

(33) Moreira, V. R.; Lebron, Y. A. R.; Foureaux, A. F. S.; Santos, L. V. D. S.; Amaral, M. C. S. Acid and Metal Reclamation from Mining Effluents: Current Practices and Future Perspectives towards Sustainability. *J. Environ. Chem. Eng.* **2021**, *9* (3), 105169. https://doi.org/10.1016/j.jece.2021.105169.

(34) Bruinsma, O. S. L.; Branken, D. J.; Lemmer, T. N.; van der Westhuizen, L.; Rossouw, S. Sodium Sulfate Splitting as Zero Brine Process in a Base Metal Refinery: Screening and Optimization in Batch Mode. *Desalination* **2021**, *511* (April), 115096. https://doi.org/10.1016/j.desal.2021.115096.

(35) Faraji, F.; Alizadeh, A.; Rashchi, F.; Mostoufi, N. Kinetics of Leaching: A Review. *Rev. Chem. Eng.* **2022**, *38* (2), 113–148. https://doi.org/10.1515/revce-2019-0073.

(36) Rodríguez De San Miguel, E.; Aguilar, J. C.; Bernal, J. P.; Ballinas, M. L.; Rodríguez, M. T. J.; De Gyves, J.; Schimmel, K. Extraction of Cu(II), Fe(III), Ga(III), Ni(II), In(III), Co(II), Zn(II) and Pb(II) with LIX® 984 Dissolved in n-Heptane. *Hydrometallurgy* **1997**, *47* (1), 19–30. https://doi.org/10.1016/s0304-386x(97)00042-x.

(37) Guimarães, A. S.; Silva, L. A.; Pereira, A. M.; Correia, J. C. G.; Mansur, M. B. Purification of Concentrated Nickel Sulfuric Liquors via Synergistic Solvent Extraction of Calcium and Magnesium Using Mixtures of D2EHPA and Cyanex 272. *Sep. Purif. Technol.* **2020**, *239* (January), 116570. https://doi.org/10.1016/j.seppur.2020.116570.

(38) Kalbe, U.; Berger, W.; Eckardt, J.; Simon, F. G. Evaluation of Leaching and Extraction Procedures for Soil and Waste. *Waste Manag.* **2008**, *28* (6), 1027–1038. https://doi.org/10.1016/j.wasman.2007.03.008.

(39) Sole, K. C.; Crundwell, F. K.; Dlamini, N.; Kruger, G. Mitigating Effects of Silica in Copper Solvent Extraction. In *9th Southern African Base Metals Conference*; The Southern African Institute of Mining and Metallurgy: Livingstone, Zambia, 2018; pp 331–342.

(40) Fletcher, A. W.; Gage, R. C. Dealing with a Siliceous Crud Problem in Solvent Extraction. *Hydrometallurgy* **1985**, *15* (1), 5–9. https://doi.org/10.1016/0304-386X(85)90062-3.

(41) Gnoinski, J. Skorpion Zinc: Optimization and Innovation. *J. South. African Inst. Min. Metall.* **2007**, *107* (10), 657–662.

(42) Choppin, G. R.; Pathak, P.; Thakur, P. Polymerization and Complexation Behavior of Silicic Acid: A Review. *Main Gr. Met. Chem.* **2008**, *31* (1–2), 53–71. https://doi.org/10.1515/MGMC.2008.31.1-2.53.

(8) Svens, K. By-Product Metals from Hydrometallurgical Processes – An Overview Kurt Svens Paper Presented at III International Conference " By-Product Metals in Non-Ferrous Metals Industry ", Wrocław , 15-17 May 2013 , Poland. **2016**, No. May 2013.

(9) Mäkinen, J.; Salo, M.; Khoshkhoo, M.; Sundkvist, J. E.; Kinnunen, P. Bioleaching of Cobalt from Sulfide Mining Tailings; a Mini-Pilot Study. *Hydrometallurgy* **2020**, *196*, 105418. https://doi.org/10.1016/j.hydromet.2020.105418.

(10) Halinen, A. K.; Rahunen, N.; Kaksonen, A. H.; Puhakka, J. A. Heap Bioleaching of a Complex Sulfide Ore: Part II. Effect of Temperature on Base Metal Extraction and Bacterial Compositions. *Hydrometallurgy* **2009**, *98* (1–2), 101–107. https://doi.org/10.1016/j.hydromet.2009.04.004.

(11) Hubau, A.; Guezennec, A. G.; Joulian, C.; Falagán, C.; Dew, D.; Hudson-Edwards, K. A. Bioleaching to Reprocess Sulfidic Polymetallic Primary Mining Residues: Determination of Metal Leaching Mechanisms. *Hydrometallurgy* **2020**, *197* (September), 105484. https://doi.org/10.1016/j.hydromet.2020.105484.

(12) Mäkinen, J.; Heikola, T.; Salo, M.; Kinnunen, P. The Effects of Milling and Ph On Co, Ni, Zn and Cu Bioleaching from Polymetallic Sulfide Concentrate. *Minerals* **2021**, *11* (3), 1–13. https://doi.org/10.3390/min11030317.

(13) Vaughan, J.; Hawker, W.; White, D. Chemical Aspects of Mixed Nickel-Cobalt Hydroxide Precipitation and Refining. In *Proceedings of the ALTA Ni/Co/Cu Conference*; 2011; pp 23–25.

(14) Liao, X.; Ye, M.; Li, S.; Liang, J.; Zhou, S.; Fang, X.; Gan, Q.; Sun, S. Simultaneous Recovery of Valuable Metal Ions and Tailings Toxicity Reduction Using a Mixed Culture Bioleaching Process. *J. Clean. Prod.* **2021**, *316* (July), 128319. https://doi.org/10.1016/j.jclepro.2021.128319.

(43) Wilhelm, S.; Kind, M. Influence of PH, Temperature and Sample Size on Natural and Enforced Syneresis of Precipitated Silica. *Polymers (Basel)*. **2015**, *7* (12), 2504–2521. https://doi.org/10.3390/polym7121528.

(44) Belton, D. J.; Deschaume, O.; Perry, C. C. An Overview of the Fundamentals of the Chemistry of Silica with Relevance to Biosilicification and Technological Advances. *FEBS J.* **2012**, *279* (10), 1710–1720. https://doi.org/10.1111/j.1742-4658.2012.08531.x.

(45) Schlesinger, M.; King, M. J.; Sole, K. C.; Davenport, W. G. *Extractive Metallurgy of Copper*, Fifth Edit.; Elsevier, Ed.; Elsevier, 2011.

(46) Tsakiridis, P. E.; Agatzini-Leonardou, S. Solvent Extraction of Aluminium in the Presence of Cobalt, Nickel and Magnesium from Sulphate Solutions by Cyanex 272. *Hydrometallurgy* **2005**, *80* (1–2), 90–97. https://doi.org/10.1016/j.hydromet.2005.07.002.

(47) Oh, C.; Han, Y. S.; Park, J. H.; Bok, S.; Cheong, Y.; Yim, G.; Ji, S. Field Application of Selective Precipitation for Recovering Cu and Zn in Drainage Discharged from an Operating Mine. *Sci. Total Environ.* **2016**, *557–558*, 212–220. https://doi.org/10.1016/j.scitotenv.2016.02.209.

(48) Lewis, A. E. Review of Metal Sulphide Precipitation. *Hydrometallurgy* **2010**, *104* (2), 222–234. https://doi.org/10.1016/j.hydromet.2010.06.010.

(49) Santanilla, A. J. M.; Aliprandini, P.; Benvenuti, J.; Tenorio, J. A. S.; Espinosa, D. C. R. Structure Investigation for Nickel and Cobalt Complexes Formed during Solvent Extraction with the Extractants Cyanex 272, Versatic 10 and Their Mixtures. *Miner. Eng.* **2021**, *160*, 106691. https://doi.org/10.1016/j.mineng.2020.106691.

(50) Bourget, C.; Soderstrom, M.; Jakovljevic, B.; Morrison, J. Optimization of the Design Parameters of a CYANEX 272 Circuit for Recovery of Nickel and Cobalt. *Solvent Extr. Ion Exch.* **2011**, *29* (5–6), 823–836. https://doi.org/10.1080/07366299.2011.595640.

(51) Saputra, R. E.; Astuti, Y.; Darmawan, A. Hydrophobicity of Silica Thin Films: The Deconvolution and Interpretation by Fourier-Transform Infrared Spectroscopy. *Spectrochim. Acta - Part A Mol. Biomol. Spectrosc.* **2018**, *199*, 12–20. https://doi.org/10.1016/j.saa.2018.03.037.

(52) Osswald, J.; Fehr, K. T. FTIR Spectroscopic Study on Liquid Silica Solutions and Nanoscale Particle Size Determination. *J. Mater. Sci.* **2006**, *41* (5), 1335–1339. https://doi.org/10.1007/s10853-006-7327-8.

(53) Almeida, R. M.; Guiton, T. A.; Pantano, C. G. Characterization of Silica Gels by Infrared Reflection Spectroscopy. *J. Non. Cryst. Solids* **1990**, *121* (1–3), 193–197. https://doi.org/10.1016/0022-3093(90)90130-E.

(54) Benesi, H. A.; Jones, A. C. An Infrared Study of the Water-Silica Gel System. *Vacuum* **1960**, *10* (3), 275. https://doi.org/10.1016/0042-207x(60)90197-4.

(55) Scott, R. P. W. The Silica-Gel Surface and Its Interactions with Solvent and Solute in Liquid Chromatography. *Faraday Symp. Chem. Soc.* **1980**, *15* (July), 49–68. https://doi.org/10.1039/FS9801500049.

(56) Katoueizadeh, E.; Rasouli, M.; Zebarjad, S. M. A Comprehensive Study on the Gelation Process of Silica Gels from Sodium Silicate. *J. Mater. Res. Technol.* **2020**, *9* (5), 10157–10165. https://doi.org/10.1016/j.jmrt.2020.07.020.

(57) Lunevich, L.; Sanciolo, P.; Smallridge, A.; Gray, S. R. Silica Scale Formation and

Effect of Sodium and Aluminium Ions -29Si NMR Study. *Environ. Sci. Water Res. Technol.* **2016**, *2* (1), 174–185. https://doi.org/10.1039/c5ew00220f.

(58) Visser, J. H. M. Fundamentals of Alkali-Silica Gel Formation and Swelling: Condensation under Influence of Dissolved Salts. *Cem. Concr. Res.* **2018**, *105* (September 2017), 18–30. https://doi.org/10.1016/j.cemconres.2017.11.006.

(59) Van Der Linden, M.; Conchúir, B. O.; Spigone, E.; Niranjan, A.; Zaccone, A.; Cicuta, P. Microscopic Origin of the Hofmeister Effect in Gelation Kinetics of Colloidal Silica. *J. Phys. Chem. Lett.* **2015**, *6* (15), 2881–2887. https://doi.org/10.1021/acs.jpclett.5b01300.

(60) Tsakiridis, P. E.; Agatzini, S. L. Process for the Recovery of Cobalt and Nickel in the Presence of Magnesium and Calcium from Sulphate Solutions by Versatic 10 and Cyanex 272. *Miner. Eng.* **2004**, *17* (4), 535–543. https://doi.org/10.1016/j.mineng.2003.12.003.

(61) Zhang, J.; Said, A.; Han, B.; Louhi-Kultanen, M. Semi-Batch Evaporative Crystallization and Drying of Cobalt Sulphate Hydrates. *Hydrometallurgy* **2022**, *208* (June 2021), 105821. https://doi.org/10.1016/j.hydromet.2022.105821.

(62) Demirel, H. S.; Svärd, M.; Uysal, D.; Doğan, Ö. M.; Uysal, B. Z.; Forsberg, K. Antisolvent Crystallization of Battery Grade Nickel Sulphate Hydrate in the Processing of Lateritic Ores. *Sep. Purif. Technol.* **2022**, *286* (January), 120473. https://doi.org/10.1016/j.seppur.2022.120473.

(63) Jenssen, I. B.; Bøckman, O.; Andreassen, J. P.; Ucar, S. The Effect of Reaction Conditions and Presence of Magnesium on the Crystallization of Nickel Sulfate. *Crystals* **2021**, *11* (12), 1–15. https://doi.org/10.3390/cryst11121485.

(64) Friesen, M.; Burt, H. M.; Mitchell, A. G. The Dehydration of Nickel Sulfate. *Thermochim. Acta* **1980**, *41* (2), 167–174. https://doi.org/10.1016/0040-6031(80)80061-X.